

*Article*

## Weight Functions for Edge Crack in Bilayer Material

Jirapong Kasivittamnuay<sup>a</sup> and Sarita Morakul<sup>b,\*</sup>

Department of Mechanical Engineering, Faculty of Engineering, Chulalongkorn University, Thailand  
E-mail: <sup>a</sup>jirapong.K@chula.ac.th (Corresponding author) , <sup>b,\*</sup>sarita.M@chula.ac.th

**Abstract.** The problem of weight functions for an edge crack in semi-infinite bilayer materials was revisited. The research aimed to develop the empirical equations for geometrical factors for reference SIFs associated with the weight functions, which covered a wider range of elastic mismatches. The weight functions in consideration covered the cases of a crack tip in a surface layer as well as in a substrate. The direct adjustment method was employed to derive the weight function coefficients. The reference SIFs for calculating the weight function coefficients were determined by finite element analysis with a systematic variation of the crack depth and the elastic mismatch parameters. The accuracies of the empirical equations for geometrical factors for the cases of a crack tip in coating and substrate were better than 1.3% and 4%, respectively. The weight functions were applied to bilayer materials with an edge crack under various crack face loading profiles. The SIFs predicted by the weight function method agreed with those from the FE method or the literature.

**Keywords:** Bilayer material, edge crack, stress intensity factor, weight function.

ENGINEERING JOURNAL Volume 27 Issue 3

Received 12 September 2022

Accepted 13 March 2023

Published 31 March 2023

Online at <https://engj.org/>

DOI:10.4186/ej.2023.27.3.37

## 1. Introduction

Bilayer materials have been used in diverse applications, such as corrosion protective coating [1], wear-resistant coating [2], and cold-spray restoration of worn or eroded parts in aircraft engines [3], as well as improvement of the strength and stiffness of aluminum alloy by the cladding of aluminum-based composite [4]. Under service loads, failure of the coating or surface layer can develop in many forms, such as interface delamination, tunneling (internal) crack, and channeling (edge) crack [5]. Edge cracking in bilayer materials becomes dominant if the tensile stress field presents in the surface layer, which may come from the mechanical load [4] or thermal load [6].

Integrity assessment of a cracked body requires a solution for a crack driving force, i.e., the stress intensity factor (SIF) or the energy release rate. There are many studies concerning the effect of various parameters, such as cracking configuration and loading type, on the mode-I SIF for edge cracking in bilayer material. The cracking configurations included edge crack in a surface layer [7-13], edge crack terminated at an interface [7-9, 13-15], and edge crack crossing an interface [7, 10, 11, 13]. The applied loadings concerned were a uniform crack face pressure [7], uniform tensile stress in a surface layer [9-11, 14, 15], linear stress distribution in a surface layer [14], remote tension [11, 13] and bending [13], and thermal transient [8, 12]. However, these SIFs are specific to loading type, which means that it is necessary to recalculate the SIF if the crack face is under an arbitrarily distributed stress. Practical methods to determine the SIF for arbitrarily distributed stress are the influence function method and the weight function (WF) method [16]. The first method, which relies on the superposition principle, is easier to implement and provides accurate SIF if a polynomial function (typically the fourth order) can accurately represent the applied stress profile. While the WF method requires much more computational effort, it has no restriction on the form of function for expressing the stress profile. Moreover, accurate representation of the thermal stress profile by a polynomial function is inefficient under a thermal (or cold) shock scenario. Therefore, the WF approach is more versatile.

Fett et al. [17] applied the direct adjustment method to derive the WFs for a single edge crack in a coating-substrate system, which covered partially cracked coating and partially cracked substrate, respectively. Determination of the WF coefficients for partially cracked coating used two reference SIFs, which were 1) uniform stress applied on the crack face and 2) concentrated force applied at the crack mouth, and the geometrical property of the crack at its mouth. For a crack that penetrated a substrate, the reference SIFs were the previous two loading cases and one additional loading case that was a concentrated force at the interface. Chen et al. applied the WF developed by Fett et al. [17] to various problems such as a semi-infinite substrate with multiple edge cracks in coating [18] and

coated cylinder with multiple axial cracks at the inner wall [19]. Eventually, they developed an empirical equation for the WF of these problems.

The crack morphology in a bilayer material depends on the Dundurs' elastic mismatch parameters and interface toughness [5]. Cracking nucleated in a coating may propagate into the substrate [2, 20-24]. Otherwise, it may arrest before reaching the interface [25] or deflect and propagate along the interface [3, 20, 22, 24]. Therefore, the application of WF for the cracking beyond the coating is also important.

This research revisited the problem of WF for a single edge crack perpendicular to an interface of an elastic isotropic bilayer material originally studied by Fett et al. [17]. The form of the WFs and the conditions for deriving their coefficients are identical to those in the literature. The main objective of this research is to develop empirical equations for the reference SIFs based on more complete cases of crack depth and a wider range of the Dundurs' elastic mismatch parameters. The present equations also included the second Dundurs' parameter since some researchers mentioned its role in the SIFs [9, 14, 15], but usually disregarded it due to its minor role. The proposed equations covered the cases of crack tip in coating and crack tip in the substrate.

## 2. Problem Description

Figure 1 illustrates the bilayer material in this study. The surface layer or coating with a thickness  $t$  is bonded to a semi-infinite substrate. The interface between two materials is abrupt and perfectly bonded. The coating has an elastic modulus and Poisson's ratio of  $E_1$  and  $\nu_1$ , respectively, and those for the substrate are  $E_2$  and  $\nu_2$ , respectively. Both layers are assumed to be homogeneous linear-elastic isotropic materials. A single edge crack with a depth of  $a$  starts from the coating. The crack tip is located either in the coating but does not reach the interface (Fig. 1(a)) or in the substrate (Fig. 1(b)). The state of stress at the crack tip is set as a plane strain. Note that the plane strain assumption is suitable for a channeling crack having a length (perpendicular to the paper) that exceeds a few times the coating thickness [5]. Furthermore, the multiple edge cracks can be treated as isolated or a single crack when the crack spacing is more than 8 times the coating thickness [26].

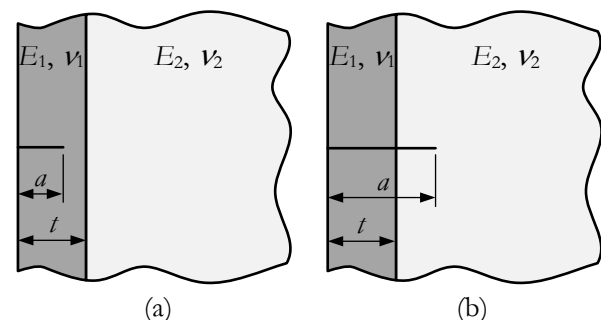


Fig. 1. Edge crack in the coating-substrate system: (a) crack tip in the coating, (b) crack tip in the substrate.

### 3. Weight Function Derivation

This section presents the derivation of the WFs for an edge crack in the bilayer material where the crack tip was in either a coating or substrate. Details for deriving the WF coefficients were presented briefly since they were almost identical to Fett et al. [17].

The pure mode-I SIF for a cracked body subjected to an arbitrarily normal stress profile can be calculated from [27]

$$K_I = \int_0^a \sigma(x) \cdot m_I(x, a) dx \quad (1)$$

where  $a$  is crack depth,  $\sigma(x)$  is normal stress distribution on the crack face (equal to the normal stress acting on the crack plane when the body is uncracked), and  $m_I(x, a)$  is the pure mode-I WF.

A general form of  $m_I(x, a)$  can be derived by substituting the analytical solution of the crack opening displacements into the definition of the WF. The derived WF is expressed as an infinite series with a singularity at the crack tip (i.e.,  $x = a$ ). However, keeping only the first 3 or 4 terms of the series is usually sufficient to provide good accuracy for SIFs determination. For the case of a crack tip in coating (Fig. 1(a)), the WF with 4 terms (3 unknown coefficients) was chosen and could be expressed as

$$m_{Ic}(x, a) = \sqrt{\frac{2}{\pi a}} \left[ (1-x/a)^{-1/2} + M_1(1-x/a)^{1/2} + M_2(1-x/a)^{3/2} + M_3(1-x/a)^{5/2} \right] \quad (2)$$

where  $M_1$ ,  $M_2$ , and  $M_3$  are the WF coefficients. For a crack tip in the substrate, i.e.,  $a > t$  (Fig. 1(b)), Fett et al. [17] found that the crack opening displacement shows a change in the slope at interface ( $x = t$ ). As a result, the derived WF shows a change in the slope at the interface. Therefore, they established the WF for each section of the crack separately, i.e.,  $0 \leq x \leq t$  and  $t < x \leq a$ , as follows:

$$m_{Ic}(x, a) = \begin{cases} \sqrt{\frac{2}{\pi a}} \left[ (1-x/a)^{-1/2} + N_1(1-x/a)^{1/2} \right] & \text{for } x > t \\ \sqrt{\frac{2}{\pi a}} \left[ N_2(1-x/a)^{-1/2} + N_3(1-x/a)^{1/2} + N_4(1-x/a)^{3/2} \right] & \text{for } x \leq t \end{cases} \quad (3)$$

where  $N_1$ ,  $N_2$ ,  $N_3$ , and  $N_4$  are the WF coefficients. The WF for a crack section in the substrate ( $x > t$ ) has only two terms. Therefore, it is suitable for a shallow crack in the substrate. For a deep crack (crack depth more than a several times the coating thickness), it is necessary to add higher-order terms like those in Eq. (2), though the determination of coefficients will be more laborious. WF for a crack section in the coating ( $0 \leq x \leq t$ ) has a similar form as Eq. (2) but has fewer terms to simplify coefficient determination. In addition, the first

coefficient ( $N_2$ ) is not set to unity to make the slope of the WF at the interface more adaptive.

Determination of the WFs coefficients  $M_i$  ( $i = 1, 2, 3$ ) and  $N_i$  ( $i = 1, 2, 3, 4$ ) requires several reference SIFs from which the crack face is subjected to a variety of simple loading cases such as uniform stress, linearly distributed stress, and point force. In some cases, the geometrical condition of the crack face profile can be used in the coefficient determination process. Once these coefficients are known, the WFs can be used to determine SIFs under arbitrarily distributed normal stress  $\sigma(x)$  acting on the crack face of the cracked body.

Three conditions for determining  $M_1$ ,  $M_2$ , and  $M_3$  consist of two reference SIFs for the problems in Fig. 2; their SIFs can be written respectively as

$$K_{1\sigma c} = \sigma \sqrt{\pi a} \cdot F_{\sigma c} \quad (4)$$

$$\text{and} \quad K_{1Pc,0} = \frac{2P}{\sqrt{\pi a}} \cdot F_{Pc,0} \quad (5)$$

where  $F_{\sigma c}$  and  $F_{Pc,0}$  are the geometrical factors for partially cracked coating under uniform stress on the crack face, and concentrated force at the crack mouth, respectively. Note that the reference SIF for the third condition is a crack face curvature of zero at its mouth, which is

$$\frac{\partial^2 m_{Ic}}{\partial x^2} = 0 \quad \text{for } x = 0 \quad (6)$$

Substituting Eqs. (2), (4), and (5) into Eq. (1) and applying the condition in Eq. (6) to Eq. (2) leads to three algebraic equations with 3 unknowns, i.e.,  $M_1$ ,  $M_2$ , and  $M_3$ . Solving these equations yields [17]

$$M_1 = -\frac{15}{4\sqrt{2}} F_{Pc,0} + \frac{35\pi}{8\sqrt{2}} F_{\sigma c} - 7 \quad (7)$$

$$M_2 = \frac{15}{2\sqrt{2}} F_{Pc,0} - \frac{35\pi}{6\sqrt{2}} F_{\sigma c} + \frac{25}{3} \quad (8)$$

$$M_3 = -\frac{7}{4\sqrt{2}} F_{Pc,0} + \frac{35\pi}{24\sqrt{2}} F_{\sigma c} - \frac{7}{3} \quad (9)$$

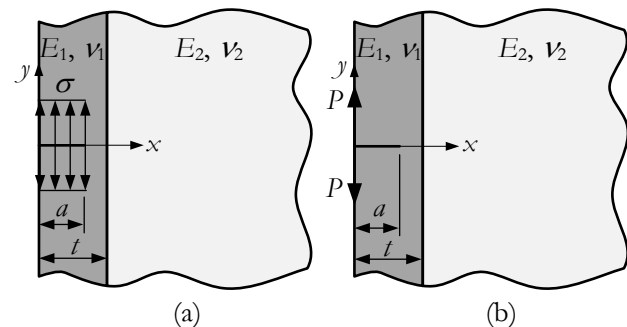


Fig. 2. Reference SIFs for  $m_{Ic}$  (Eq. (2)). (a) uniform stress on the crack face, (b) concentrated force on the crack mouth.

Determination of  $N_1$ ,  $N_2$ ,  $N_3$ , and  $N_4$  requires four conditions. The first three conditions are reference SIFs for the problems in Fig. 3, which can be expressed as

$$K_{1\sigma_s} = \sigma \sqrt{\pi a} \cdot F_{\sigma_s} \quad (10)$$

$$K_{1P_{s,0}} = \frac{2P}{\sqrt{\pi a}} \cdot F_{P_{s,0}} \quad (11)$$

and

$$K_{1P_{s,t}} = \frac{2P}{\sqrt{\pi a}} \cdot F_{P_{s,t}} \quad (12)$$

where  $F_{\sigma_s}$ ,  $F_{P_{s,0}}$  and  $F_{P_{s,t}}$  are the geometrical factors for substrate cracking under uniform stress on the crack face, concentrated force at the crack mouth, and concentrated force at the interface, respectively. The fourth condition is each part of the WF in Eq. (3) requiring the same value at  $x = t$  or satisfying the  $C_0$  continuity condition.

Substituting Eqs. (3), (10) - (12) into Eq. (1) and applying the  $C_0$  continuity condition leads to a system of equations with 4 unknowns, i.e.  $N_1$ ,  $N_2$ ,  $N_3$ , and  $N_4$ . Solving these equations yield the WF coefficients as shown in Eqs. (13) - (16). All coefficients except for  $N_4$  are identical to the results by Fett et al. [17] but are expressed in different forms. The coefficient  $N_4$  was corrected for the misprint in the original work.

$$N_1 = \sqrt{\frac{2}{1-\gamma}} F_{P_{s,t}} - \frac{1}{1-\gamma} \quad (13)$$

$$N_2 = \frac{(1-\gamma)}{R_4} \left\{ \begin{array}{l} (1 + \sqrt{1-\gamma}) [R_3 - (2-\gamma)R_2] \\ -\frac{R_1}{2} (1 - \sqrt{1-\gamma}) \left[ \begin{array}{l} 6\sqrt{1-\gamma} + 4(1-\gamma) \\ +2(1-\gamma)^{3/2} + 3 \end{array} \right] \end{array} \right\} \quad (14)$$

$$-\frac{R_2}{R_4} \sqrt{1-\gamma}$$

$$N_3 = \frac{1}{R_4} \left\{ (\gamma - 2)(1 + \sqrt{1-\gamma}) [R_3 - (1-\gamma)R_2] \right. \\ \left. + \frac{3}{2} R_1 (1 - \sqrt{1-\gamma}) \left[ \begin{array}{l} 2\sqrt{1-\gamma} + 3(1-\gamma) \\ +4(1-\gamma)^{3/2} + 1 \end{array} \right] \right. \\ \left. + 6R_2 \sqrt{1-\gamma} \right\} \quad (15)$$

$$N_4 = \frac{1}{R_4} \left[ (1 + \sqrt{1-\gamma}) \left( R_3 - \frac{5}{2} R_1 \right) \right. \\ \left. - 5\sqrt{1-\gamma} (R_2 - R_1 \sqrt{1-\gamma}) \right] \quad (16)$$

with  $\gamma = \frac{t}{a}$  (17)

$$R_1 = \sqrt{2} F_{P_{s,0}} \quad (18)$$

$$R_2 = \sqrt{2} F_{P_{s,t}} \quad (19)$$

$$R_3 = \frac{15\pi}{4\sqrt{2}} F_{\sigma_s} - 5\sqrt{1-\gamma} \quad (20)$$

$$R_4 = -\gamma \left[ \gamma^2 + \sqrt{1-\gamma} - 2(1-\gamma) + (1-\gamma)^{3/2} \right] \quad (21)$$

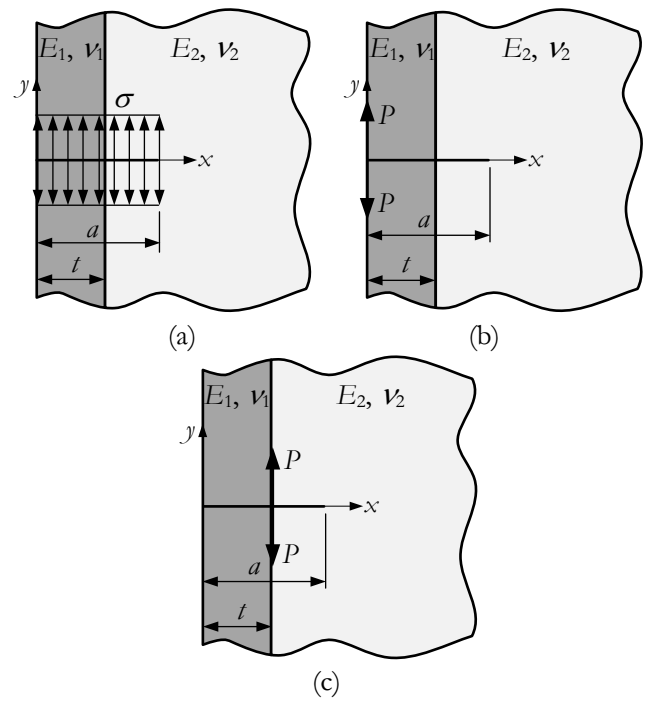


Fig. 3. Reference SIFs for  $m_s$  (Eq. (3)). (a) uniform stress on the crack face, (b) concentrated force on the crack mouth, (c) concentrated force at the interface.

## 4. Finite Element Analysis

### 4.1. Finite Element Model and Post-Processing

The finite element (FE) method was used to calculate five reference SIFs for the problems shown in Figs. 2 and 3, i.e.  $K_{1\sigma_s}$ ,  $K_{1P_{s,0}}$ ,  $K_{1\sigma_s}$ ,  $K_{1P_{s,0}}$ , and  $K_{1P_{s,t}}$ . These SIFs were then used to determine the corresponding geometrical factors,  $F_{\sigma_s}$ ,  $F_{P_{s,0}}$ ,  $F_{\sigma_s}$ ,  $F_{P_{s,0}}$ , and  $F_{P_{s,t}}$  by Eqs. (4), (5), (10) - (12), respectively. The analysis model shown in Fig. 4(a) was the upper half of the body due to symmetrical geometry and loading. This half-model has a width  $W$  and height  $H$  of 20 times the coating thickness to sufficiently represent the semi-infinite substrate. The uncracked ligament (i.e., a line from crack tip to point A) was restrained in the  $y$ -direction. Further, point A was restrained in the  $x$ -direction.

The domain was divided into 3 zones as shown in Fig. 4(b): internal zone (area 1), transition zone (areas 2 and 4), and external zone (areas 3, 5, 6). The entire domain was discretized by the 8-node quadrilateral element. The mesh sizes in the internal, transition and external zones were kept below 0.5 mm, 0.5 mm, and 4 mm respectively. The crack tip was encompassed with 12 elements of a quarter-point singularity element with a size of  $t/100$ . Figure 4(c) shows an example of the FE mesh created from this setting. The chosen crack-tip mesh size was derived from the mesh convergence studied for the case of  $E_2/E_1 = 1/50$ ,  $\nu_1 = 0.4$ , and  $\nu_2 = 0.1$  as shown in Table 1. The results indicated that a crack tip mesh size of  $t/100$  or finer was sufficient.

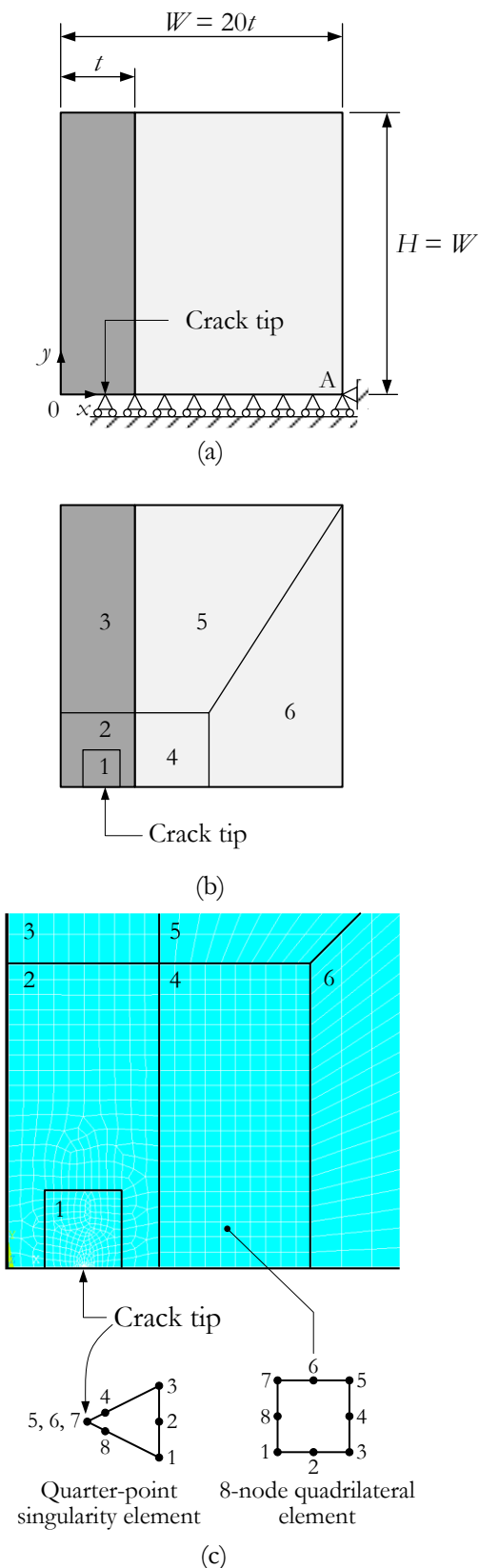


Fig. 4. FE model for edge cracking in the coating-substrate system. (a) domain of the problem to be analyzed by the FE, (b) partitioning of the domain for setting mesh size, (c) FE mesh (the numbers shown are the area numbers in Fig. 4(b)).

Table 1. Effect of crack tip mesh size on the SIFs for an edge crack in bilayer material with  $E_2/E_1 = 1/50$ ,  $\nu_1 = 0.4$ , and  $\nu_2 = 0.1$ .

$a/t$	Crack tip mesh size	SIF ( $\text{MPa}\sqrt{\text{mm}}$ )	Convergence rate (%)
0.1	$t/50$	2.0680	-
	$t/100$	2.0649	0.15
	$t/150$	2.0608	0.20
	$t/200$	2.0647	0.19
0.9	$t/50$	18.247	-
	$t/100$	18.222	0.14
	$t/150$	18.208	0.08
	$t/200$	18.178	0.17
1.1	$t/50$	5.3378	-
	$t/100$	5.3308	0.13
	$t/150$	5.3219	0.17
	$t/200$	5.3052	0.31

The FE analysis cases are summarized in Table 2. Seven values of an elastic modulus ratio were chosen from 50 to 1/50. The Poisson's ratio of coating and substrate varied from 0.1 to 0.4. The relative crack depth was divided into 2 groups: from 0.1 to 0.9 for the crack tip in the coating, and from 1.1 to 1.5 for the crack tip in the substrate. The relative crack depth varied with a step of 0.1 for both groups. The total number of analyses is 3,696 cases.

For all analysis cases, the coating thickness  $t$  was set to 10 mm, while the applied stress and applied concentrated force were set to 1 MPa and 1 N/mm, respectively. Additionally, both coating and substrate were assumed to be isotropic linear-elastic material.

ANSYS Mechanical APDL 2022 R1 was used in the FE modeling and analysis. A two-dimensional plane strain linear-elastic stress analysis was performed. The SIF was extracted from the FE solution by a displacement extrapolation method.

Table 2. FE analysis cases.

$E_2/E_1$	$\nu_1$	$\nu_2$	$a/t$	
			crack tip in coating	crack tip in substrate
50, 10, 3, 1, 1/3, 1/10, 1/50	0.1, 0.2, 0.3, 0.4	0.1, 0.2, 0.3, 0.4	0.1, 0.2, ..., 0.9	1.1, 1.2, ..., 1.5

## 4.2. Validation of the Finite Element Model

Preliminary FE analyses were carried out to evaluate the FE model. The analysis cases covered  $a/t = 0.6, 0.9, 1.1$ , and  $1.5$ ,  $\nu_1 = \nu_2 = 0.3$ , and all values of  $E_2/E_1$  listed in Table 2. The SIFs of the present analyses were close to those in the literature [17]. The maximum difference percentage was less than 0.7%, as shown in Fig. 5. Therefore, the present FE models were suitable.

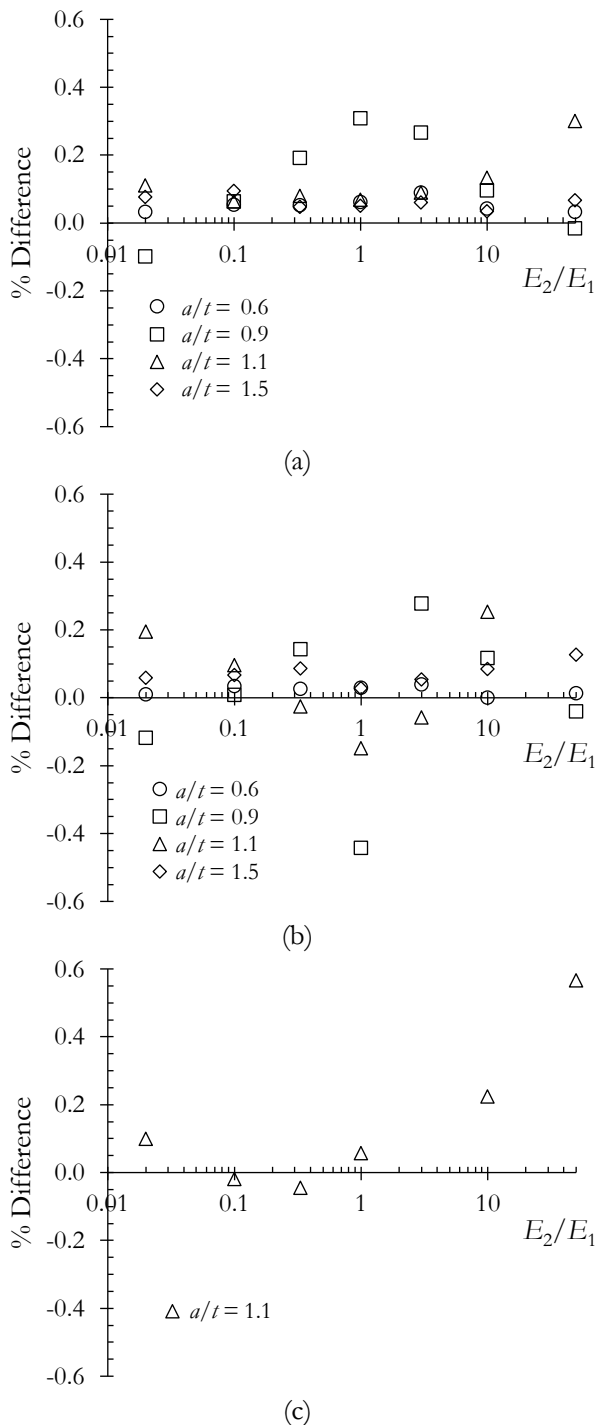


Fig. 5. Percentage difference between the geometrical factors from the present analysis and those from the literature [17]. (a) crack face under uniform stress, (b) concentrated force at the crack mouth, (c) concentrated force at the interface.

### 4.3. Development of the Empirical Equations for the Geometrical Factors

The dimensional analysis by Chen et al. [18] suggested that the geometrical factors of the reference problems are dependent on the relative crack depth  $a/t$  and Dundurs' parameters,  $\alpha$  and  $\beta$ . These parameters in a plane strain condition are defined as:

$$\alpha = \frac{(1-\nu_2^2) - (1-\nu_1^2)(E_2/E_1)}{(1-\nu_2^2) + (1-\nu_1^2)(E_2/E_1)} \quad (22)$$

$$\beta = \frac{(1-2\nu_2)(1+\nu_2) - (1-2\nu_1)(1+\nu_1)(E_2/E_1)}{2[(1-\nu_2)^2 + (1-\nu_1)^2(E_2/E_1)]} \quad (23)$$

The analysis cases listed in Table 2 are expressed in terms of parameters  $\alpha$  and  $\beta$  covering  $-0.97 \leq \alpha \leq 0.97$  and  $-0.43 \leq \beta \leq 0.43$ .

The proposed empirical equations of the geometrical factors for the case of crack tip in coating (Eqs. (4) and (5)) and those for the crack tip in a substrate (Eqs. (10) – (12)) were adapted from the originals proposed by Bueth [9], and Chakravarthy et al. [11], respectively. Modifications were done to include the effect of the mismatch parameter  $\beta$ , and to improve the fitting accuracy of the equations to the FE results.

For the crack tip in the coating, i.e.  $0.1 \leq a/t \leq 0.9$ , the following equations are proposed.

$$F_{\sigma_c} = 1.1215(1-\gamma^{-1})^{0.5-s} \left[ 1 + \sum_{k=0}^2 \sum_{j=0}^3 \sum_{i=0}^4 A_{ijk} s^i (1+\beta)^{j-1.5} \gamma^{-(k+1)} \right] \quad (24)$$

$$F_{P_{c,0}} = 1.2967(1-\gamma^{-1})^{0.5-s} \left[ \sum_{i=0}^1 B_i s^i + \sum_{k=0,1,3} \sum_{j=0}^3 \sum_{i=0}^4 C_{ijk} s^i (1+\beta)^{j-1.5} \gamma^{-(k+1)} \right] \quad (25)$$

For the crack tip in the coating, i.e.  $1.1 \leq a/t \leq 1.5$ , the following equations are proposed.

$$F_{\sigma_s} = \sqrt{\frac{4}{\pi^2 - 4}} (1-\gamma)^{0.5-s} \arcsin(\gamma) \left[ \sum_{i=0}^2 D_i s^i + \sum_{k=0}^1 \sum_{j=0}^2 \sum_{i=0}^4 E_{ijk} s^i (1+\beta)^{j-0.5} \gamma^{k+1} \right] \quad (26)$$

$$F_{P_{s,0}} = \sqrt{\frac{4}{\pi^2 - 4}} (1-\gamma)^{0.5-s} \arcsin(\gamma) \left[ (1+\beta)^{0.5} \sum_{i=0}^4 F_i s^i + \sum_{k=0,2} \sum_{j=0}^4 G_{ijk} s^i (1+\beta)^{j-0.5} \gamma^{k+1} \right] \quad (27)$$

$$F_{P_{s,t}} = \sqrt{\frac{4}{\pi^2 - 4}} (1-\gamma)^{0.5-s} \arcsin(\gamma) \left[ (1+\beta)^{0.5} \sum_{i=0}^4 H_i s^i + \sum_{k=0,2} \sum_{j=0}^4 I_{ijk} s^i (1+\beta)^{j-0.5} \gamma^{k+1} \right] \quad (28)$$

where  $A, B, C, D, E, F, G, H,$  and  $I$  are the array of the best-fit coefficients obtained from a multivariate regression analysis,  $\gamma = t/a$  (as defined in Eq. (17)), and  $s$  is the stress singularity exponent, which is the root of the following equation [9].

$$\cos(s\pi) - 2\frac{\alpha - \beta}{1 - \beta}(1 - s)^2 + \frac{\alpha - \beta^2}{1 - \beta^2} = 0 \quad (29)$$

The procedure for determining the best fit coefficients, such as  $A_{ijk}$  in Eq. (24), can be described as follows. First, calculate the SIFs for the problem in Fig.

2(a),  $K_{I\sigma}$  with the conditions listed in Table 2 by the FE method. Next, determine the values of  $F_{\sigma}$  for each  $K_{I\sigma}$  by Eq. (4). After that, calculate parameters  $\alpha$  and  $\beta$  from  $E_2/E_1$ ,  $\nu_1$  and  $\nu_2$  by Eqs. (22) and (23). Finally, import  $F_{\sigma}$ ,  $\alpha$ ,  $\beta$ , and  $\gamma$  into the MathCAD Prime 8 software and perform the regression analysis. Tables 3 to 7 list the best-fit coefficients obtained. The accuracies of Eqs. (24) – (28) compare with the FE results are better than 0.9%, 1.3%, 1.5%, 2.3%, and 4%, respectively.

Table 3. Coefficients of the empirical equation for the geometrical factor  $F_{\sigma}$  (Eq. (24)).

$k$	$i$	$A_{ijk}$			
		$j$			
		0	1	2	3
0	0	4.8865	-25.4751	48.8633	-33.2935
	1	-15.2483	94.9360	-215.0581	166.8609
	2	16.1409	-100.7910	309.6607	-299.7752
	3	-35.0998	79.6141	-208.8431	244.6504
1	4	32.3761	-54.9130	68.8265	-79.4798
	0	-36.5509	200.7467	-361.1774	207.2366
	1	79.6998	-628.2291	1458.1433	-987.8293
	2	-28.0480	523.4710	-2001.0707	1718.5527
2	3	81.1248	-190.2061	1205.6737	-1348.9960
	4	-110.2435	124.1796	-313.7367	414.9449
	0	24.2550	-128.8949	230.8651	-136.0420
	1	-55.6501	405.5752	-932.7804	655.7398
3	2	26.8595	-331.0126	1252.7566	-1141.4175
	3	-81.0580	159.6001	-763.1977	906.7430
	4	96.8566	-130.8647	223.7142	-288.7359

Table 4. Coefficients of the empirical equation for the geometrical factor  $F_{P_{c,0}}$  (Eq. (25)).

$i$	$B_i$	$C_{ijk}$					
		$k$	$i$	$j$			
				0	1	2	3
0	1.0275	0	0	19.0042	-101.7768	183.5547	-111.7888
1	-0.0273	0	1	-56.3407	365.5792	-771.0650	530.1137
			2	64.1121	-478.6774	1200.3620	-949.6167
			3	-49.5032	294.4525	-831.4210	764.9828
			4	29.7273	-95.0480	228.6693	-236.6782
		1	0	-80.5426	453.7541	-811.2871	446.8636
			1	172.4072	-1414.5759	3224.2902	-2070.4955
			2	-71.6850	1377.1876	-4624.9992	3596.6285
			3	35.5982	-447.0268	2854.1250	-2795.7066
		3	4	-80.3586	82.9863	-666.3432	830.2146
			0	54.3746	-316.8078	570.0624	-305.1604
			1	-85.2698	878.2308	-2159.3524	1384.4429
			2	-34.6238	-601.5770	2860.0163	-2331.5436
		4	3	7.2397	6.3162	-1618.7219	1773.2048
			4	78.2386	-9.8951	368.7876	-527.2779

Table 5. Coefficients of the empirical equation for the geometrical factor  $F_{\sigma}$  (Eq. (26)).

$i$	$D_i$	$E_{ijk}$				
		$k$	$i$	$j$		
				0	1	2
0	10.9567	0	0	4.2422	-103.1045	128.1222
1	-16.0751		1	4.4829	351.9856	-597.2399
2	9.6613		2	-82.2304	-362.0835	1022.0642
			3	121.8876	51.0429	-760.6885
			4	-51.0440	57.7858	208.2549
		1	0	-51.1111	220.7396	-181.8729
			1	215.5994	-1038.1141	926.7782
			2	-276.9919	1753.4198	-1738.2612
			3	99.3837	-1253.4351	1428.9510
			4	16.0106	317.7855	-436.0319

Table 6. Coefficients of the empirical equation for the geometrical factor  $F_{P_{x,0}}$  (Eq. (27)).

$i$	$F_i$	$G_{ijk}$				
		$k$	$i$	$j$		
				0	1	2
0	6.1290	0	0	-31.4746	47.4532	45.0332
1	39.3730		1	211.9490	-516.7770	-151.7083
2	-151.5983		2	-441.5656	1430.8199	116.9440
3	179.3637		3	368.5585	-1558.7133	56.8419
4	-70.4549		4	-104.1129	593.3145	-67.7559
		2	0	-13.2217	65.8405	-81.4684
			1	10.2444	-204.8346	400.6762
			2	86.6974	99.9885	-689.7583
			3	-173.5417	200.7294	493.2629
			4	89.6570	-162.7823	-121.8989

Table 7. Coefficients of the empirical equation for the geometrical factor  $F_{P_{x,t}}$  (Eq. (28)).

$i$	$H_i$	$I_{ijk}$				
		$k$	$i$	$j$		
				0	1	2
0	84.2572	0	0	99.5929	-509.5828	286.5160
1	-281.7385		1	-402.7792	2235.0275	-1480.3848
2	320.0753		2	531.5109	-3554.0392	2814.7186
3	-99.0316		3	-222.5514	2355.8109	-2344.1899
4	-22.5653		4	-6.4540	-525.7468	723.8191
		2	0	-354.6015	1145.4594	-606.5143
			1	1661.1774	-5983.0802	3429.3230
			2	-2593.2307	11319.8448	-7051.6559
			3	1471.2994	-9188.1268	6292.5491
			4	-171.1898	2696.1879	-2065.6293

#### 4.4. Application of the Weight Functions

This section demonstrates the application of the derived WF and the empirical equations for the geometrical factors of the reference SIFs to the example problems, as shown in Fig. 6. Three cases of stress profiles acted on the crack face consisting of uniform stress  $\sigma(x) = 1$  MPa, linear decreasing stress  $\sigma(x) = [1 - (x/a)]$  MPa, and complementary error function  $\sigma(x) = \text{erfc}(x/t)$  MPa, where  $x$  is the distance along the crack

plane measured from the crack mouth. The first problem (Fig. 6(a)), and the second problem (Fig. 6(b)) included the cases of crack tips in coating and substrate. The third problem (Fig. 6(c)), which resembles a thermal shock condition [5, 17] was concerned only with the case of crack tip in coating and with  $a/t = 0.8$ . Table 8 lists the chosen elastic mismatch parameters for these problems.

Table 8. Values of the elastic mismatch parameters for the example problems (Fig. 6).

Case	Problems 1 and 2		Problem 3	
	$\alpha$	$\beta$	$\alpha$	$\beta$
1	-0.97	-0.43	-0.96	-0.27
2	-0.79	-0.10	-0.82	-0.23
3	-0.56	-0.31	-0.50	-0.14
4	0.08	0.16	0.00	0.00
5	0.56	0.31	0.50	0.14
6	0.79	0.10	0.82	0.23
7	0.97	0.43	0.96	0.27

The SIFs for each stress profile were calculated by Eq. (1). The WF used depends on the location of the crack tip. For the crack tip in the coating, the WF in Eq. (2) was used. Otherwise, Eq. (3) was used. The proposed empirical equations for the geometrical factors (i.e., Eqs. (24) – (28)) were used to calculate the associated WF coefficients.

Figures 7 and 8 show the plot of the SIFs obtained by the WF and FE methods at different relative crack depths for problems 1 and 2, respectively. These plots illustrated the agreement of the SIFs determined by both methods. The distribution of the percentage difference for the WF results from the FE results is shown in Fig.

9(a) and 9(b) for problems 1 and 2, respectively. The percentage difference for the first problem was mostly within  $\pm 1\%$ , whereas the difference mostly lied within  $-3\%$  to  $1\%$  for the second problem. For the third problem, the present SIFs by WF and FE results from the literature [17] are shown in Table 9. The percentage difference in the table indicated the agreement between both methods.

Table 9. SIFs for the edge crack in bilayer material subjected to complementary error function stress profile on the crack face (problem 3) by the WF and FE methods.

Case	SIF ( $\text{MPa}\sqrt{\text{mm}}$ )		% Difference
	WF	FE [17]	
1	1.7876	1.7988	-0.61
2	1.9268	1.9331	-0.34
3	2.2670	–	–
4	2.9433	2.9338	0.32
5	4.0851	–	–
6	5.7827	5.7532	0.51
7	8.4172	8.4448	-0.33

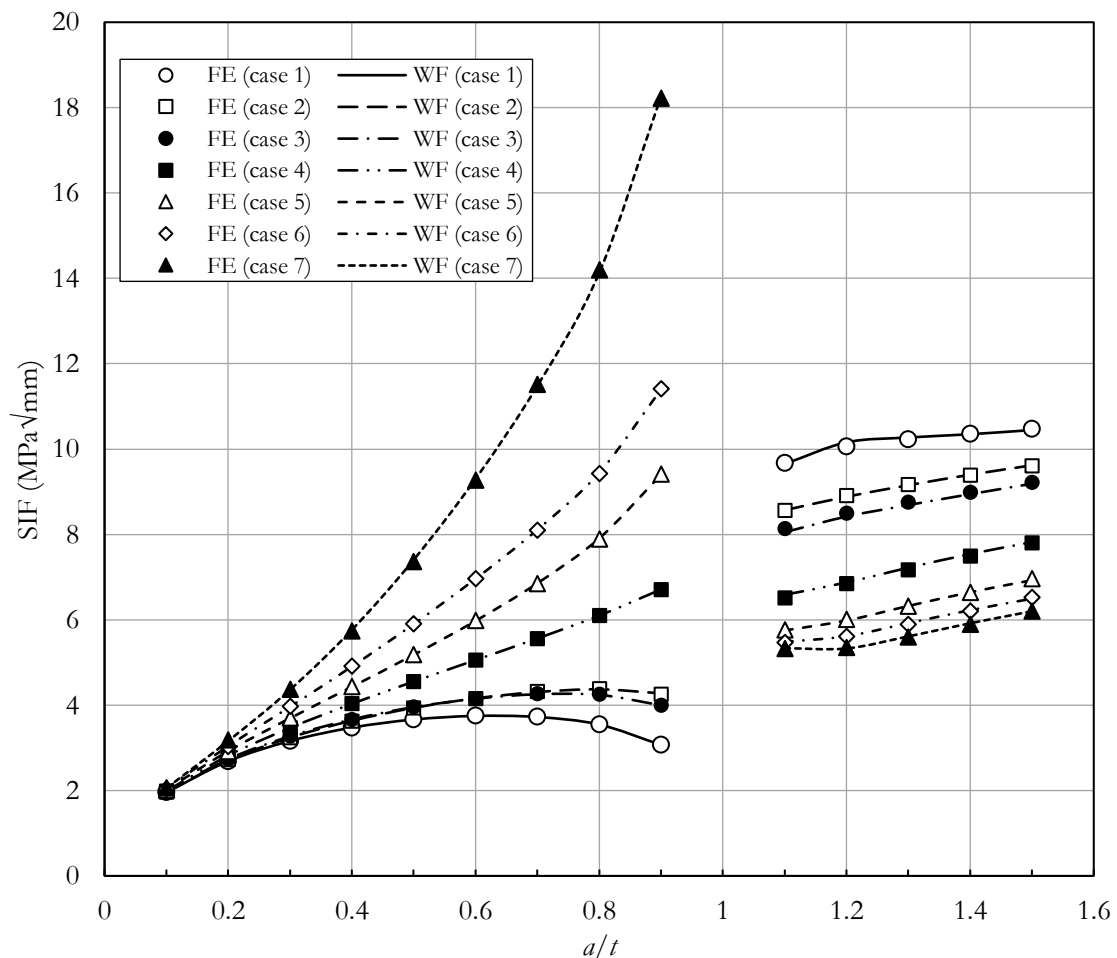


Fig. 7. SIFs for the edge crack in bilayer material subjected to uniform stress profile on the crack face (problem 1) by the WF and FE methods.

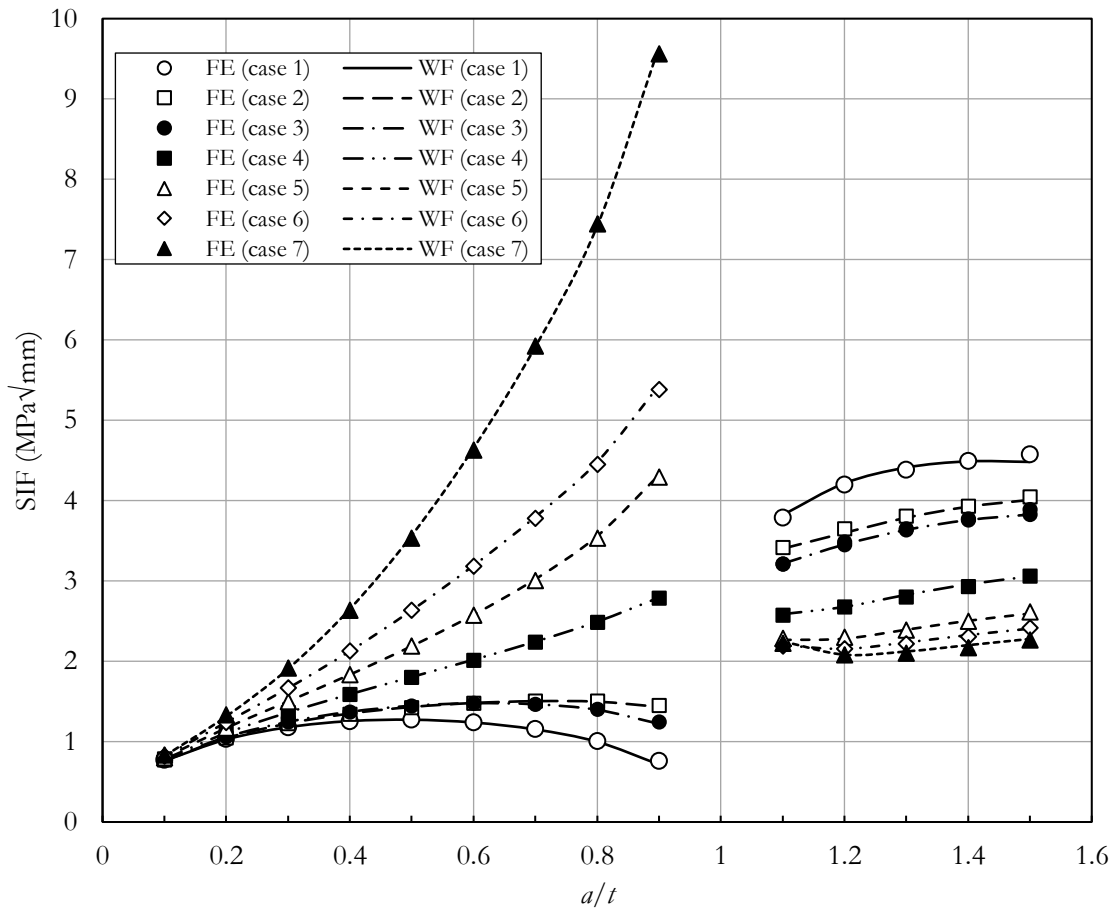


Fig. 8. SIFs for the edge crack in bilayer material subjected to linear decreasing stress profile on the crack face (problem 2) by the WF and FE methods.

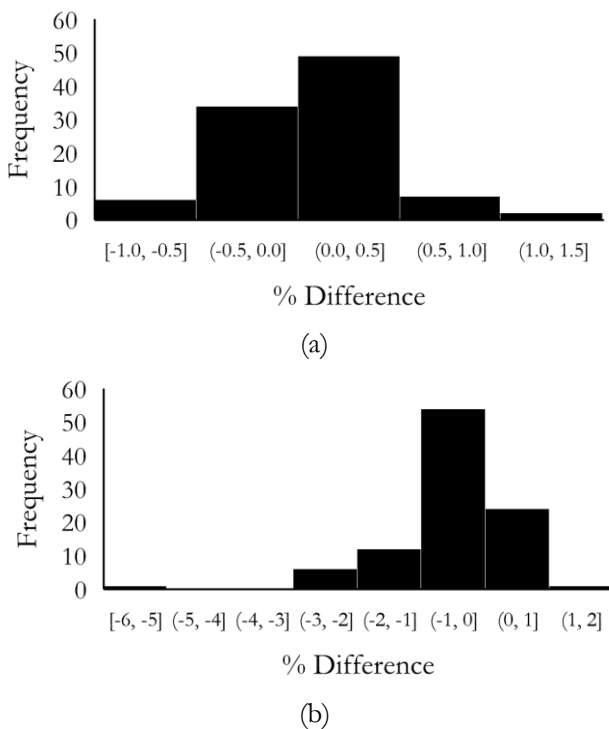


Fig. 9. Histogram of the percentage difference in the prediction of SIFs by the WF method from those calculated by the FE method. (a) Problem 1, (b) Problem 2.

## 5. Discussion

It has already been shown that the SIFs determined by the WF method were reasonably accurate. It is useful to suggest a further application of the derived WFs and the associated empirical equations for the geometrical factors, such as the problem of fatigue crack growth (FCG) life prediction in residual stress field. In this problem, the WF is used to calculate the SIF due to the residual stress and then combined with the SIF due to the applied load to determine the effective SIF range, which is a governing parameter of the FCG rate. The FCG life can be calculated by integrating the inverse of the FCG rate equation from an initial crack size to a final crack size. The details of employing the WF in FCG life prediction in a residual stress field can be found in the literature (e.g. [28]). However, the present study did not cover the relative crack depth between  $0.9 < a/t < 1.1$ . The analysis of the FCG life for a crack that grows from a coating surface to some distance in the substrate must be separated into 2 intervals: the first interval from an initiation depth to  $a/t = 0.9$  and the second interval from  $a/t = 1.1$  to a final depth. This approximation yields a conservative FCG life since the FCG life from  $a/t = 0.9$  to 1.1 was omitted. Future works on the development of the small-scale-yielding or elastic-plastic crack tip parameters might be beneficial.

## 6. Conclusions

The problem of weight functions (WFs) for edge cracking in linear elastic isotropic bilayer material was revisited. The direct adjustment method was employed in the derivation of the WF coefficients as done by Fett et al. [17]. The study included the WFs for partially cracked coating and partially cracked substrate. One of the WF coefficients in the literature was corrected. The reference SIFs for calculation of the WF coefficients were determined using linear-elastic FE analysis in plane strain. The analysis cases systematically varied the relative crack depth from 0.1 to 0.9 and 1.1 to 1.5. The elastic mismatch parameters were also systematically varied from the Dundurs' parameters from  $\alpha = -0.97$  to 0.97 and  $\beta = -0.43$  to 0.43, which almost completed their theoretical ranges (i.e.,  $\alpha = \pm 1$  and  $\beta = \pm 0.5$ ). The empirical equations for the geometrical factors for the associated reference SIFs were proposed. Accuracies of the empirical equations as compared with the FE results for the cases of crack tip in coating and substrate were better than 1.3% and 4%, respectively. The WFs were applied to the bilayer material with edge crack under different crack face loadings, i.e., the uniform stress profile, linear decreasing stress profile, and complementary error function profile. The SIFs calculated by the WF method conformed to those determined by the FE method or from the literature.

## Acknowledgement

This research did not receive any specific grant from funding agencies in the public, commercial, or not-for-profit sectors.

## References

- [1] M. A. Eder, P. U. Haselbach, and O. V. Mishin, "Effects of coatings on the high-cycle fatigue life of threaded steel samples," *J. Mater. Eng. Perform.*, vol. 27, pp. 3184-3198, 2018.
- [2] Y. Feng, X. Pang, K. Feng, Y. Feng, and Z. Li, "Residual stress distribution and wear behavior in multi-pass laser cladded Fe-based coating reinforced by  $M_3(C,B)$ ," *J. Mater. Res. Technol.*, vol. 15, no. 5, pp. 5597-5607, 2021.
- [3] A. W. Y. Tan, W. Sun, A. Bhowmik, J. Y. Lek, I. Marinescu, F. Li, N. W. Khun, Z. Dong, and E. Liu, "Effect of coating thickness on microstructure, mechanical properties and fracture behavior of cold sprayed Ti6Al4V coating on Ti6Al4V substrate," *Surf. Coat. Technol.*, vol. 349, pp. 303-317, 2018.
- [4] A. A. Iqbal, Y. Arai, and W. Araki, "Influence of residual stress on the fatigue crack growth mechanism in the Al-alloy/Hybrid MMC Bi-Material," *J. Fail. Anal. Prev.*, vol. 22, 2022. [Online]. Available: <https://doi.org/10.1007/s11668-022-01432-7>
- [5] M. R. Begley and J. W. Hutchinson, *The Mechanics and Reliability of Films, Multilayers and Coatings*. UK: Cambridge University Press, 2017.
- [6] X. Chen and X. Wang, "Effects of substrate thickness and heat transfer scheme on edge cracking of brittle coating due to thermal transients," *Theor. Appl. Fract. Mech.*, vol. 90, pp. 100-109, 2017.
- [7] M. C. Lu and F. Erdogan, "Stress intensity factors in two bonded elastic layers containing cracks perpendicular to and on the interface—II Solution and results," *Eng. Fract. Mech.*, vol. 18, no. 3, pp. 507-528, 1983.
- [8] A. A. Rizk, "Stress intensity factor for an edge crack in two bonded dissimilar materials under convective cooling," *Theor. Appl. Fract. Mech.*, vol. 49, pp. 251-267, 2008.
- [9] J. L. Beuth, "Cracking of thin bonded films in residual tension," *Int. J. Solids Struct.*, vol. 29, no. 13, pp. 1657-1675, 1992.
- [10] T. Ye, Z. Suo, and A. G. Evans, "Thin film cracking and the roles of substrate and interface," *Int. J. Solids Struct.*, vol. 29, no. 21, pp. 2639-2648, 1992.
- [11] S. S. Chakravarthy, E. H. Jordan, and W. K. S. Chiu, "Thin film and substrate cracking under the influence of externally applied loads," *Eng. Fract. Mech.*, vol. 72, no. 8, pp. 1286-1298, 2005.
- [12] X. Chen, Q. Liu, and Q. Ma, "A parametric investigation on thermally driven edge cracking of a coating-substrate system," *J. Coat. Technol. Res.*, vol. 9, pp. 541-549, 2012.
- [13] N. A. Noda, K. Araki, and F. Erdogan, "Stress intensity factors in two bonded elastic layers with a single edge crack under various loading conditions," *Int. J. Fract.*, vol. 57, pp. 101-126, 1992.
- [14] J. J. Vlassak, "Channel cracking in thin films on substrates of finite thickness," *Int. J. Fract.*, 119, pp. 299-323, 2003.
- [15] M. Keikhaie, N. Keikhaie, R. Keikhaie, and M. M. Kaykha, "Stress intensity factors in two bonded elastic layers containing crack perpendicular on the interface with different elastic properties," *J. Mod. Phys.*, vol. 6, no. 5, pp. 640-647, 2015.
- [16] T. L. Anderson, *Fracture Mechanics: Fundamentals and Application*, 3rd ed. Boca Raton: CRC Press, 2005.
- [17] T. Fett, E. Diegele, D. Munz, and G. Rizzi, "Weight functions for edge cracks in thin surface layers," *Int. J. Fract.*, vol. 81, pp. 205-215, 1996.
- [18] X. Chen and Y. You, "Weight functions for multiple edge cracks in a coating," *Eng. Fract. Mech.*, vol. 116, pp. 31-40, 2014.
- [19] X. Chen and Y. You, "Weight functions for multiple axial cracks in a coated hollow cylinder," *Arch. Appl. Mech.*, vol. 85, pp. 617-628, 2015.
- [20] T. Tanaka and M. Hori "The propagation of the fatigue crack crossing the interface of metal composites under the effect of residual thermal stress," *Bull. JSME*, vol. 22, no. 172, pp. 1359-1367, 1979.

- [21] S. Suresh, Y. Sugimura, and T. Ogawa, "Fatigue cracking in materials with brittle surface coating," *Scripta Metall. Mater.*, vol. 29, no. 2, pp. 237-242, 1993.
- [22] T. Guo, L. Qiao, X. Pang, and A. A. Volinsky, "Brittle film-induced cracking of ductile substrates," *Acta Mater.*, vol. 99, pp. 273-280, 2015.
- [23] H. M. Espejo and D. F. Bahr, "Substrate cracking in Ti-6Al-4V driven by pulsed laser irradiation and oxidation," *Surf. Coat. Technol.*, vol. 322, pp. 46-50, 2017.
- [24] S. T. Alweendo, M. Morita, K. Hasegawa, and S. Motoda, "Fatigue properties of hot-dip galvanized AISI 1020 normalized steel in tension-compression and tension-tension loading," *Materials*, vol. 14, p. 7480, 2021.
- [25] S. Zak and R. Pippin, "Cracks in thin Cu films on Si substrate – Plasticity influence," *Theor. Appl. Fract. Mech.*, vol. 110, p. 102809, 2020.
- [26] F. Delannay and P. Warren, "On crack interaction and crack density in strain-induced cracking of brittle films on ductile substrates," *Acta Metall. Mater.*, vol. 39, no. 6, pp. 1061-1072, 1991.
- [27] T. L. Anderson, *Fracture Mechanics: Fundamentals and Applications*. Taylor & Francis, 2005.
- [28] N. Kashaev, S. Keller, P. Staron, E. Maawad, and N. Huber, "On the prediction of fatigue crack growth based on weight functions in residual stress fields induced by laser shock peening and laser heating," *Fatigue Fract. Eng. Mater. Struct.*, vol. 44, pp. 3463-3481, 2021.



Jirapong Kasivitanuay received his B. Eng. and M. Eng. degrees from Chulalongkorn University, and doctoral degree in mechanical engineering from The University of Tokyo. Since 2000, he has been a faculty member at the Department of Mechanical Engineering, Chulalongkorn University. At present, he is an associate professor. His research interest is fracture mechanics, fatigue, and development of a classroom demonstration rigs for the mechanics of materials course.



**Sarita Morakul** received her B. Eng. Degrees from Thamaasat university, Thailand, Master degree of mechanical engineering from Nagaoka university of technology, Japan, and doctoral degree in material science of engineering from Nagaoka university of technology, Japan. Since 2020, she has been a faculty member at Department of Mechanical Engineering, Chulalongkorn University. At present, she is lecturer and interesting research topic is fracture mechanics and fatigue, coating and interfacial surface, and biomaterials.